

# Plasmonic Systems Unveiled by Fano Resonances

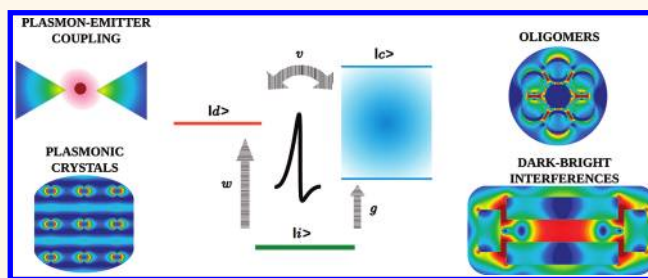
Yan Francescato, Vincenzo Giannini,\* and Stefan A. Maier

The Blackett Laboratory, Imperial College London, London SW7 2AZ, United Kingdom

One of the main features of plasmonics and also one of its greatest successes is the reshaping of a nanosystem's response to light.<sup>1</sup> Such design has allowed among other achievements single molecule detection<sup>2–4</sup> and nanolasing,<sup>5</sup> it is also widely used in spectroscopy<sup>6–10</sup> and as a way to control emitters.<sup>11</sup> In this context, Fano interferences are a powerful tool to alter a resonance in a very small frequency range. Here, the interaction between a discrete state and a continuum gives rise to resonant suppression and enhancement of scattering in a narrow frequency window, and typical asymmetric line shapes result.<sup>12</sup> The literature on Fano interferences is vast, and the interested reader is referred to the reviews by Miroshnichenko<sup>13</sup> and Luk'yanchuk<sup>14</sup> for a bird's view on the matter. In plasmonics, Fano profiles have been reported for quite some time in surface-enhanced infrared absorption (SEIRA)<sup>15</sup> in which a molecular absorption line interacts with the localized surface plasmon resonances (LSPR) of metallic nanostructures.<sup>16–18</sup> Interferences between dark and bright resonances are also very common and can be observed, for example, in dolmen geometries;<sup>19–22</sup> sometimes a Fano resonance can only be revealed by symmetry breaking, such as the one induced by mirror charges in a substrate<sup>23–26</sup> or by misaligning multi-component nanocavities.<sup>27–30</sup> However, in most situations, the line shapes are caused by interferences between plasmonic modes with different lifetimes, as in nanoshells<sup>31,32</sup> and oligomers.<sup>33–39</sup> Finally, Fano resonances are crucial for such schemes as plasmon emitters<sup>40,41</sup> and within the sensing community, where higher-order<sup>42</sup> and magnetic resonances in nanoclusters<sup>43</sup> or the LSPR of complex nanocavities<sup>44,45</sup> are studied.

As can be seen, Fano interferences are omnipresent in state-of-the-art nanophotonics, and this is well acknowledged by a strong impulse in providing new theoretical developments of Fano theory applied to the

## ABSTRACT



We show in detail how a derivation of Fano theory can serve as a new paradigm to study, understand, and control the interaction of nano-objects with light. Examples include a plasmonic crystal, a dolmen-type structure sustaining dark and bright plasmon modes, and a nanoshell heptamer. On the basis of only three coupling factors, a straightforward analytical formula is obtained, only assuming a plasmonic resonance for the continuum, and retaining the nonclassical character of the original formalism. It allows one to predict, reproduce, or decompose Fano interferences solely in terms of the physical properties of the uncoupled nanostructures when available, without the need of additional fitting parameters.

**KEYWORDS:** plasmonic Fano resonances · oligomers or nanoclusters · dark and bright modes · dolmen · EIT · lattice resonances · plasmonic crystals

particular case of plasmonics.<sup>18,46–51</sup> Nevertheless, these recasts of Fano's original work are usually phenomenological descriptions, classical in nature and quite far from Fano's formalism.

We propose in what follows a unified point of view on nanoscale interference phenomena by means of a derivation of Fano theory presented earlier.<sup>18</sup> The only assumption regards the continuum state line shape, which is described as a plasmonic resonance, and the final expression simplifies to an analytic formula based on three coupling parameters and a set of properties that are strictly related to the uncoupled system. In a second stage, we analyze some particular cases in light of our formula. First, there is a plasmonic crystal composed of 2D periodically arranged spheres, where the interaction happens between the spheres' Mie resonances and the in-plane scattered light. Second, a symmetric nanostructure

\* Address correspondence to v.giannini@imperial.ac.uk.

Received for review December 23, 2011 and accepted January 26, 2012.

Published online 10.1021/nn2050533

© XXXX American Chemical Society

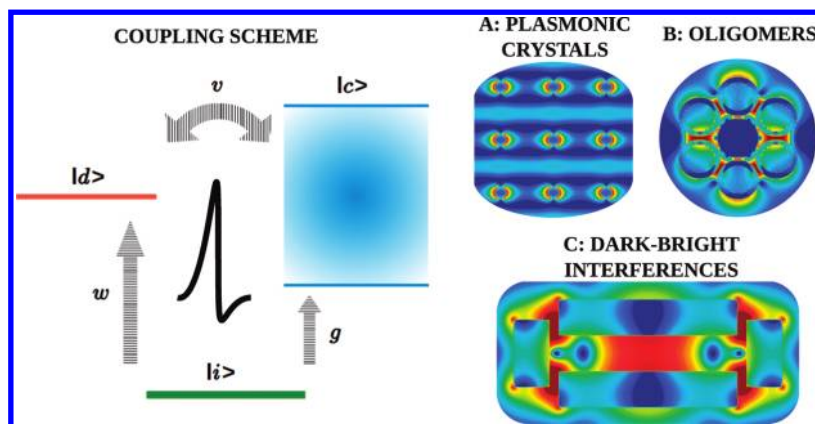


Figure 1. Left: schematic of a Fano resonance, an incident photon  $|i\rangle$  excites either a discrete mode  $|d\rangle$  with a coupling factor  $w$  or the continuum  $|c\rangle$  with coupling factor  $g$ , both interacting via a coupling strength  $\nu$ . Right: case of Fano interferences discussed in the present work.

that displays an electromagnetically induced-like transparency (EIT) is studied. Last, nanoshells forming a highly symmetric heptamer in which the buildup of a sub- and a super-radiant mode arises due to the hybridization of the individual particles.

We show how a reasonable estimate of the coupling factors can be acquired from general physical considerations; such factors are central to describing the various plasmonic situations analytically. Of particular interest is the deep physical insight that can be attained through this procedure. To the contrary of most past approaches, where the profile is numerically fitted to a Fano line shape, here there are no floating parameters. In the end, let us stress that this formulation of Fano theory proves quite powerful also for further designing plasmonic nanostructures, and as soon as good coupling strengths are found analytically, further fine-tuning of the optical response of such systems can follow.

**Analytic Fano Profile.** When two states are spectrally close, they can interact and give rise to a so-called Fano line shape, where destructive and constructive interferences take place in a very narrow frequency range. Often, these profiles are asymmetric, in which case they display the most typical signature of a Fano resonance. In a previous work,<sup>18</sup> we showed how within the original frame of Fano theory one can deduce an analytic formula that describes the interaction between a sharp state,  $|d\rangle$ , and a broad resonance,  $|c\rangle$ , when excited by an incident photon,  $|i\rangle$  (see Figure 1, left). The parameter that expresses the direct interaction between the narrow and broad resonances is the coupling factor  $\nu$ , while  $w$  and  $g$  give, respectively, the probability to directly excite the discrete or the continuum state (see Figure 1, left). The spectrum,  $F$ , beautifully recovers the same form as the original Fano profile (eq 1a), but now its ingredients,  $\mathcal{G}$ , the reduced energy, and  $q$ , the excitation probability ratio (also called asymmetry parameter), are not unidentified quantities any more; they are clear and simple analytic

functions of the plasmonic and discrete states deriving naturally from the theory (eqs 1b and 1c)

$$F(\mathcal{G}) = \frac{(\mathcal{G}+q)^2}{\mathcal{G}^2+1} \quad (1a)$$

$$q = \frac{\nu w/g}{\Gamma_m(E)/2} + \frac{E - E_P}{\Gamma_P/2} \quad (1b)$$

$$\mathcal{G} = \frac{E}{\Gamma_m(E)/2} - \frac{E - E_P}{\Gamma_P/2} \quad (1c)$$

Here  $E$  is the energy of the incoming photon and  $E_P$  and  $\Gamma_P$  are the energy and line width of the broad plasmonic resonance, which has a Lorentzian line shape given by

$$\mathcal{L}(E) = \frac{1}{1 + \left(\frac{E - E_P}{\Gamma_P/2}\right)^2} \quad (2)$$

The energy of the sharp state  $E_d$  is taken at the origin, and its modified line width is written as  $\Gamma_m(E) = 2\pi\nu^2\mathcal{L}(E)$ .

The coupling factors  $\nu$ ,  $g$ , and  $w$  are usually unknown; however, the main idea of the present paper is to show that each parameter can be related to physical properties of the noninteracting system. Such a description is almost exact in the case of emitters coupled to plasmonic nanostructures,<sup>18</sup> and it can be extended to the situation of plasmon–plasmon interactions with very good results. It is important to note though that a strong coupling strength between nanostructures can affect the original noninteracting resonances. Our approach allows then to understand how the interference is occurring and which parameters are critical. It can in turn be a powerful tool to alter a system's response to light, being either resonant suppression or enhancement of scattering of interest.

## RESULTS AND DISCUSSION

**Plasmonic Crystals.** As a first example, we will consider a plasmonic crystal composed of 2D periodically arranged metallic nanoparticles in a dielectric environment

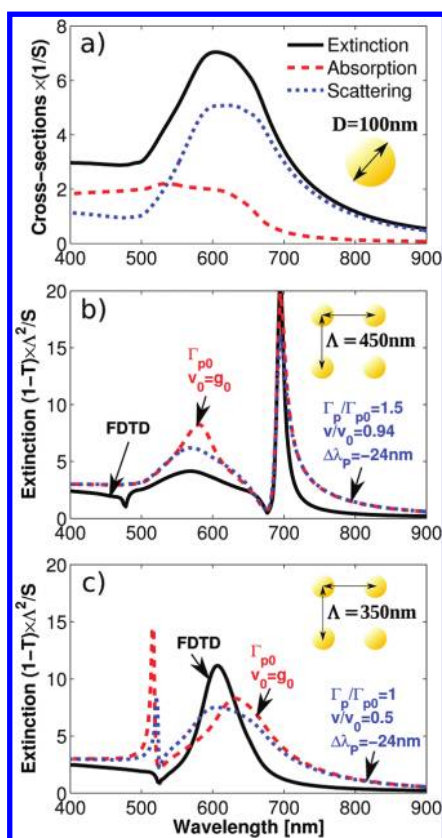


**Figure 2.** (a) Normalized (to  $S = \pi \times R^2$ ) extinction (solid black line), scattering (dotted blue line), and absorption (dashed red line) cross sections of a 50 nm radius gold sphere calculated by FDTD. (b,c) Normalized (to  $S/\Lambda^2$ ) extinction ( $1 - T$ ) of the same nanoparticle arranged periodically along  $X$  and  $Y$  with  $\Lambda =$  (b) 450 nm and (c) 350 nm. The solid black lines are FDTD results, and dashed red lines are obtained by  $\text{Ext} = \sigma_{\text{scat}} \times F(\zeta) + \sigma_{\text{abs}}$  with  $F(\zeta)$  from eqs 1. All of the parameters are taken from the single sphere cross sections with  $g_0 = (\Gamma_p/2\pi)^{1/2}$ ,  $v_0 \sim g_0$ , and  $w \sim 0$ . For the dotted blue curves,  $E_p$ ,  $\Gamma_p$ , and  $v$  have been slightly amended to show better accordance with the FDTD results (see plots for full details).

with  $n = 1.5$ . Such a system has experienced a recent increase in interest because of its ability to exhibit very sharp and strong features due to what is known as lattice resonances.<sup>52–58</sup> These are given by the interference of the LSPR (broad state) with the in-plane scattered light at the Rayleigh anomaly position (discrete state). Here we analyze gold spheres having a radius of 50 nm (inset of Figure 2a) and a periodicity  $\Lambda$  of 450 nm (inset of Figure 2b) and 350 nm (inset of Figure 2c); each case is simulated by FDTD with experimental data for the dielectric function.<sup>59</sup> To get a physical insight into the interaction, we shall use the optical properties of a single sphere as a starting point which can be described by the absorption,  $\sigma_{\text{abs}}$ , scattering,  $\sigma_{\text{scat}}$ , and extinction,  $\sigma_{\text{ext}} = \sigma_{\text{scat}} + \sigma_{\text{abs}}$ , cross sections shown in Figure 2a. The magnitude  $\sigma_{\text{scat}}$  has two contributions, the strongest is the excitation of the LSPR centered around 620 nm, which is the collective oscillation of the electrons of the metallic sphere

making it an efficient radiative antenna; the weakest is the elastic Rayleigh scattering that determines the scattering behavior at longer wavelengths. While  $\sigma_{\text{abs}}$  is caused by ohmic losses. In order to compare similar quantities, the extinction of the single sphere is normalized to its physical cross section  $S = \pi \times R^2$ , while the array extinctions, expressed as  $1 - T$ , are normalized by  $S/\Lambda^2$ . In the array case (see Figure 2b), the sharp peak at about 700 nm is caused by the Fano interference between the Rayleigh anomaly at the diffraction condition  $k_{\parallel} = 2\pi/n\Lambda$  and the LSPR.

We will now show how to use eqs 1 to describe this interference process. From the isolated sphere (Figure 2a), we can obtain  $E_p$  and  $\Gamma_p$  that are given by the line width and position of  $\sigma_{\text{scat}}$ . Furthermore, the extinction of an array can be written in the usual Fano way (see Methods section), that is,  $\text{Ext} = \sigma_{\text{scat}} \times F(\zeta) + \sigma_{\text{abs}}$ , or in other words the scattering of a single particle modified by an interaction term given by the Fano interference. The absorption is an incoherent process that does not participate directly in the interference but adds as a background in the resulting profile. The coupling parameter,  $g_0$ , the excitation of the plasmonic resonance by the incoming photons, depends on the LSPR width and is expressed as  $g_0 = (\Gamma_p/2\pi)^{1/2}$ .<sup>18</sup> The interaction factor  $v_0$  between the two states is unknown but will be chosen similar to  $g_0$  as a first approximation. The diffracted wave traveling along the interface originates from the cooperative Rayleigh scattering of the particles. However, as said already, this contribution to  $\sigma_{\text{scat}}$  is very small compared to the LSPR, hence  $w_0$ , which characterizes the direct excitation of the discrete state, is much smaller than the other coupling factors and is taken as null.

Figure 2 shows the extinction of our plasmonic crystals as calculated by FDTD (solid black curves) and with the Fano formulation (eqs 1) developed in this paper with the aforementioned values for the various parameters (red dashed curves) and slightly tuned to show a better accordance (blue dotted curves). As can be seen from the  $\Lambda = 450$  nm case (Figure 2b), the agreement is very good even without any fitting, which clearly shows that the proposed coupling parameters are relevant to reproducing the physics of the coupled systems. Note that we are only considering the interferences between two states; the second-order diffraction dip at higher energy (Figure 2b, at around 480 nm) is by consequence not taken into account. This is a demonstration of all the potential of our approach since we only used known properties of the uncoupled structures to predict the line shape produced by the interaction process.

Nevertheless, if we now look at the  $\Lambda = 350$  nm spectrum (Figure 2c), the formula forecasts a peak while there is only a dip. Actually, in this case, the plasmonic resonance is at lower energy than the diffracted wave, and it has been shown that there is

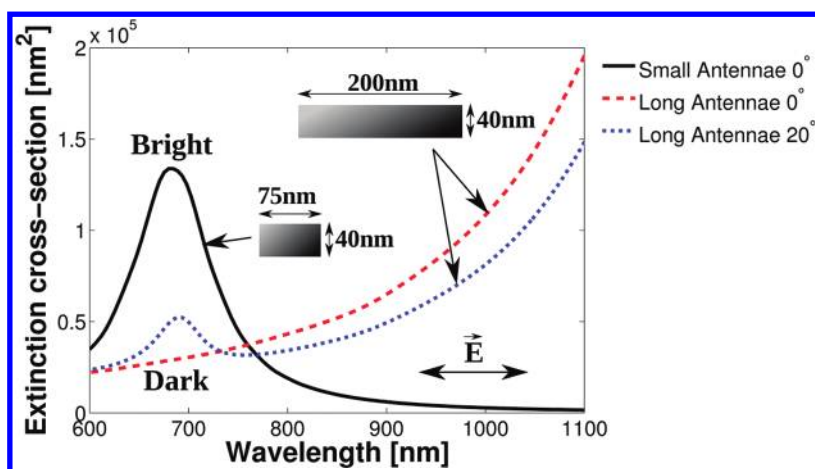


Figure 3. Extinction cross sections of the long (dashed red line) and short (solid black line) antennae pairs at normal incidence. The dipolar resonance of the latter is matched to the second-order resonance of the former that can only be excited when the symmetry is broken, here *via* a tilted illumination of  $20^\circ$  (dotted blue). The long antennae also support a dipolar mode that is located in the near-infrared which explains the increase of their extinction toward longer wavelength.

little radiative interaction.<sup>54</sup> Additionally, because of non-negligible absorption, the Fano modulation is hardly observed.<sup>21,27,50</sup> In other words, we are assuming that an interference is fully taking place while it is barely present. Even here the analysis remains useful because the discrepancy tells us that the observed extinction is not due to a Fano resonance.

**Dark-Bright Plasmonic Interference.** Let us now turn to a system which allows us to explore the interaction between a dark and a bright plasmon resonance. As a matter of fact, composite structures like dolmens have arisen as fascinating geometries to observe an optical switching phenomenon very similar to electromagnetically induced transparency (EIT).<sup>18–22,60,61</sup>

The studied structure is composed of two perpendicular pairs of metallic antennae which are designed such that the first-order resonance (referred to subsequently as dipolar) of the short beams is spectrally matched to the second-order resonance of the long beams. The extinction cross sections of these antennae pairs are plotted in Figure 3; they consist of beams of 75 nm (solid black line) and 200 nm (red dashed and blue dotted curves) long, respectively, with a cross section of  $40 \times 40 \text{ nm}^2$ . They are made out of silver, and the dielectric function in FDTD was taken from experiments,<sup>62</sup> with the background refractive index set to  $n = 1.5$ . Our goal is to predict the spectra of the complex interacting system only from the knowledge of the properties of the simple noninteracting components. One can see that the second-order mode can only be observed away from normal incidence (see dotted blue line in Figure 3 with  $\theta = 20^\circ$ , for example) because it is symmetry-forbidden otherwise.

By assembling the two pairs of beams in a symmetric fashion (the lateral distance between the long beams is 40 nm; see inset of Figure 4a) with light polarized perpendicular to the long antennae, we guarantee that their second-order resonance excitation can only

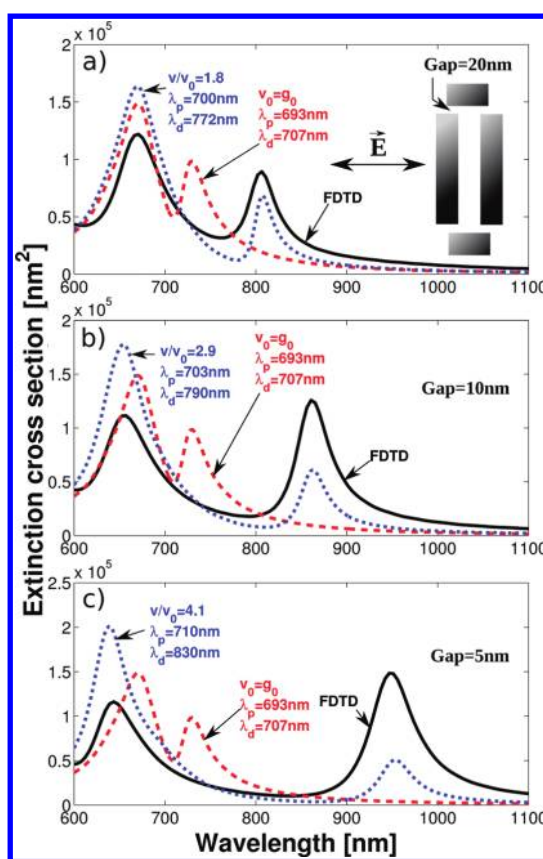
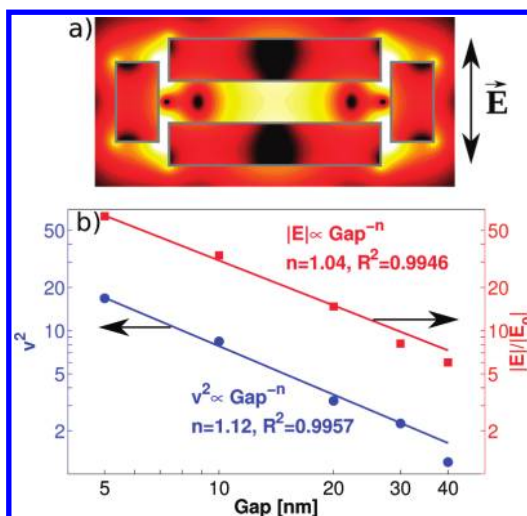


Figure 4. Extinction cross sections of the dolmen structure for a gap  $G = 20 \text{ nm}$  (a),  $10 \text{ nm}$  (b), and  $5 \text{ nm}$  (c). The solid black lines are FDTD calculations, and the dashed red curves are obtained by  $\text{Ext} = \sigma_{\text{scat}} \times F(\mathcal{L}) + \sigma_{\text{abs}}$  with  $F(\mathcal{L})$  from eqs 1. All of the parameters are taken from the cross sections of the uncoupled antenna pairs with  $g_0 = (\Gamma_p/2\pi)^{1/2}$ ,  $v_0 \sim (\Gamma_d/2\pi)^{1/2}$ , and  $w = 0$ . For the dotted blue curves,  $E_d$ ,  $E_p$ , and  $v$  have been modified to fit the FDTD results (see plots for full details).

be driven from the near-field of the short antennae dipolar resonances. Figure 4 shows the resulting extinction spectra (full black lines) for a varying gap  $G$

between the long antennae tip and the short antennae side ranging from  $G = 20$  nm (Figure 4a), 10 nm (Figure 4b), and 5 nm (Figure 4c) as calculated by FDTD; note how the splitting between the two modes arising from interferences is strongly affected by  $G$ . In the same way as for the plasmonic crystal previously, let us write again  $\text{Ext} = \sigma_{\text{scat}} \times F(\zeta) + \sigma_{\text{abs}}$  for the extinction of the full structure (see Methods section). From Figure 3, we have all of the information about the noninteracting system. Since the resonances of the longer antennae are dark, the only contribution to the extinction is from the bright mode. Hence there remain only the coupling factors  $g$ ,  $\nu$ , and  $w$ , as well as the widths and energy positions of the resonances necessary in  $F(\zeta)$  (see eqs 1). The energy positions  $E_p$  and  $E_d$  and line widths  $\Gamma_p$  and  $\Gamma_d$  are taken, respectively, from  $\sigma_{\text{scat}}$  of the dipolar resonance of the small antenna pair (solid black curve, Figure 3) and the second-order mode of the long pair (dotted blue curve, Figure 3). The direct excitation of the second-order resonance in the longer antenna is forbidden, hence  $w_0 = 0$ . Next, as in the previous case,  $g_0$  is linked to the bright mode width via  $g_0 = (\Gamma_p/2\pi)^{1/2}$ .<sup>18</sup> For  $\nu_0$ , we use the same approximation, writing it at first as  $(\Gamma_d/2\pi)^{1/2}$ . However, it should be pointed out that  $\nu_0$  depends on the gap because it expresses the coupling between the dark mode in the longer antennae with the bright mode in the short ones; considering  $\nu_0$  independent of the gap is therefore a rough estimate. The dashed red curves present the profiles obtained with the parameters just described: we can see that for bigger gaps the approximated value of  $\nu_0$  works quite well, but it fails to predict the position of the second peak and the dispersion due to variations of the gap. For this reason, a study of  $\nu_0$  for different gap sizes will be useful to gain insight into the interference mechanism. We can appreciate a very good agreement in Figure 4 for the dotted blue curves, which represent the case where  $\nu_0$ ,  $E_p$ , and  $E_d$  have been modified in order to reproduce the numerical calculations. Note that the small changes in  $E_p$  and  $E_d$  in Figure 2 and Figure 4 are caused by the mutual influence of the different components within the nanostructure when placed in the near-field of each other, resulting in a small deviation from the independent isolated plasmonic modes.

As mentioned,  $\nu_0$  has to depend on the gap; indeed, when the antennae are closer, a stronger interaction is expected between the dark and the bright resonances, as can be seen from the electric intensity near-field plot in Figure 5a. Since the coupling between the two modes is taking place through near-field interactions, a similar behavior of the electric field in the gaps can be expected. For this reason, it is instructive to report the values of the coupling factor  $\nu$  (from the dotted blue lines in Figure 4) and the electric field amplitude  $E$  calculated from FDTD against the gap width (Figure 5b). Interestingly,  $\nu^2$  is indeed revealed to follow a very



**Figure 5.** (a) Near-field cut at midheight of the nanostructure shown in the inset of Figure 4a with  $G = 10$  nm showing the electric field intensity at 860 nm on a logarithmic scale (the outline of the structure is drawn in gray). (b) Coupling factor  $\nu^2$  and electric amplitude,  $|E|$ , in the middle of the gap at the second peak in function of the gap  $G$  on a log–log scale. The blue and red lines represent the fits  $\nu^2 = 103 \times G^{-1.12}$  and  $|E| = 339 \times G^{-1.04}$  with correlation coefficient  $R^2 = 0.9957$  and  $0.9946$ , respectively.

similar trend than the electric field amplitude  $|E|/|E_0|$  calculated in the gap between the antennae. More precisely, they are almost inversely proportional to the gap width  $G$  (see Figure 5b).

**Nanocluster.** The last problem we will consider is that of plasmon hybridization in metal nanoclusters; in particular, we will explore the case of a heptamer of gold nanoshells (see inset of Figure 6). These kinds of nanoclusters have attracted the attention of researchers as strongly coupled nanostructures, where the large interaction gives rise to the formation of a sub- and a super-radiant mode.<sup>63</sup> In particular, the theory of hybridization in plasmonics was first developed to explain the complex spectra of systems composed out of nanoshells.<sup>31</sup> It has since been used to describe most cases of composite objects, including nanocavities<sup>28–30</sup> and oligomers.<sup>33–39</sup>

The hybridization theory combined with the presented model can provide key information on the interfering plasmonic resonances when a Fano resonance is present. For example, we can decompose an experimental spectrum of a nanocluster system into the original modes that are interfering, as we will show in what follows. This is very important because if we know the “original resonances” of the nanoparticles composing the nanocluster that sustain them, we can understand how to manipulate and improve the design of such structure.

We consider now a heptamer embedded in a dielectric disk with  $n = 1.5$  and dimensions [height, radius] = [10 nm, 85 nm]; see inset of Figure 6, similar to the designs shown in ref 35. The inner and outer

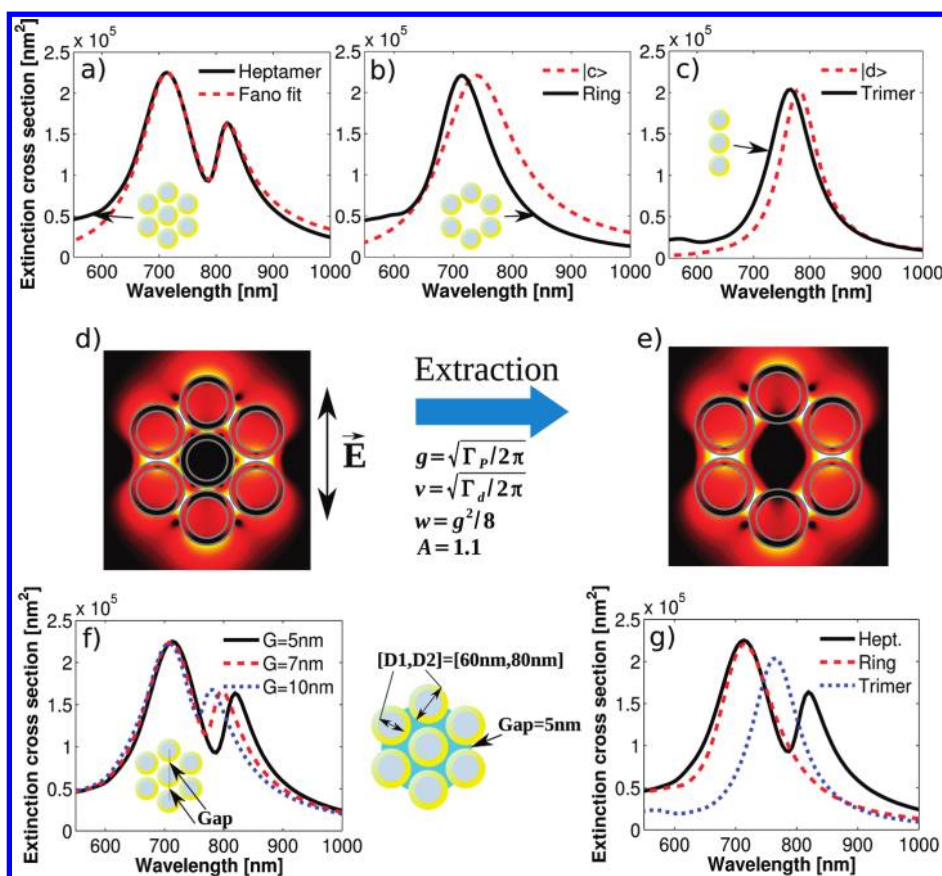


Figure 6. (a–c) Solid black lines are the extinction cross sections calculated by FDTD of (a) a full heptamer of gold nanoshells, (b) its external ring, and (c) the vertical trimer (see respective insets). The dashed red curves represent (a) the fit obtained with the analytic Fano formula  $F'(E)$  with  $A$  linked to absorption (see eqs 1 and Methods section) and its extracted (b) bright  $|c\rangle$  and (c) dark  $|d\rangle$  modes (see Methods section). (d,e) FDTD near-field cuts at midheight at 713 nm in log scale of (d) the full heptamer and (e) its external ring. (f) FDTD extinction cross sections of the full heptamer by varying the two gaps  $G$  along the vertical trimer axis (polarization direction) from  $G = 5$  nm (solid black curve) to 7 nm (dashed red line) and 10 nm (dotted blue curve). (g) Suggested original modes for the heptamer structure (solid black line): a bright mode originating from the ring resonance (red dashed curve) and a dark state with a strong trimer character (dotted blue curve).

radius of the nanoshells are  $[R_1, R_2] = [30 \text{ nm}, 40 \text{ nm}]$ ; the core is silica, and the gaps between closest neighbors are set to 5 nm.

Figure 6a shows the FDTD extinction spectrum (Ext) of the proposed structure (solid black line), and the dashed red curve is what can be obtained with the analytic formula  $F'(E) = g^2 \mathcal{L} \times (F(\mathcal{L}) + A)$ , with  $A$  linked to absorption (see eqs 1 and Methods section). This profile is calculated by minimizing the error  $|CF'(E) - \text{Ext}|$ , where the normalization constant  $C$  is simply fixing the units, leaving all parameters ( $E_p$ ,  $\Gamma_p$ ,  $E_d$ ,  $\Gamma_d$ ,  $w$ , and  $A$ ) free to vary since we have no prior knowledge of the two modes interacting. Here the procedure is different from the two previous problems where good coupling parameters could be estimated by general physical considerations. In the present situation, we use the known FDTD profile to retrieve the two “original” resonances. This means we assume Lorentzian line shapes for the bright and the dark modes. The coupling factors  $g$  and  $\nu$  then read  $g = (\Gamma_p/2\pi)^{1/2}$  and  $\nu = (\Gamma_d/2\pi)^{1/2}$ .<sup>18</sup> Here  $A$  is taken as constant; however, this approximation can be improved by considering

more complex functions; also, for big particles such as the ones studied in the present case, the scattering is clearly dominant. The parameters  $E_p$ ,  $\Gamma_p$  and  $E_d$ ,  $\Gamma_d$  that minimize the error  $|CF'(E) - \text{Ext}|$  are the positions and line widths of the interfering bright and dark modes resulting from the decomposition of the Fano fit (see Methods section). The extracted bright mode  $|c\rangle$  with  $E_p$  and  $\Gamma_p$  is shown in Figure 6b (dashed red line), while the original dark mode  $|d\rangle$  with  $E_d$  and  $\Gamma_d$  is shown in Figure 6c (dashed red line).

Furthermore, a near-field plot of the complete heptamer at the first peak (see Figure 6d) reveals a field distribution that seems to leave out the central nanoshell; if one calculates the near-field of an empty arrangement, without the central shell (see inset of Figure 6b), at its main resonance the field certainly does look similar to the full structure (see Figure 6e). This suggests that one of the modes is formed by the nanocluster without the central component, as confirmed by observation from Hentschel *et al.*<sup>42</sup> and Lassiter and co-workers.<sup>64</sup> In fact, it is remarkable to note (see Figure 6b) that the extracted bright mode  $|c\rangle$

(dashed red line) is rather close to the spectrum of this external ring (solid black line). In addition, as expected, the state is red-shifted and broadened due to the interaction with the central particle.

Subradiant modes cannot be perfectly isolated because they are dark, and we are exciting the nanostructure with a plane wave. However, crucial information can also be gathered by means of eqs 1. Both Hentschel *et al.*<sup>42</sup> and Lassiter and co-workers<sup>64</sup> observed that the central particle plays a fundamental role in the formation of the subradiant mode in heptamers. Additionally, we find that the upper and lower particles along the polarization axis do also strongly participate in the dark resonance. Indeed altering this central trimer (see inset of Figure 6c,f) along the vertical axis by varying the two gaps  $G$  (see Figure 6f) from  $G = 5$  nm (solid black curve) to 7 nm (dashed red line) and 10 nm (dotted blue curve) shows an appreciable shift of the Fano interference while marginally affecting the first peak at 713 nm, which is mostly of bright mode character. Therefore, the vertical trimer contributes significantly to the dark state. We also expect the dipolar moment of this trimer to be antiparallel to that of the lateral nanoshells in the subradiant mode. In Figure 6c, we can see the trimer extinction (solid black curve) alongside the extracted dark mode  $|d\rangle$  (dashed red line) which indeed share similar properties. Following this analysis, we therefore propose (see Figure 6g) that the extinction of the full heptamer structure

(full black curve) is the result of the Fano interference between a super-radiant mode originating from the ring resonance (dashed red curve) and a subradiant mode with a strong trimer character (dotted blue curve).

## CONCLUSION

In conclusion, we have shown *via* a detailed study of three different problems, plasmonic crystals, dark-bright plasmons interaction, and nanocluster modes how the nonclassical derivation of the original Fano theory can lead to an analytic description of most interference phenomena encountered in plasmonics.

Different resonances were considered, including localized surface plasmons and diffractive modes, bright and dark states, as well as built-in sub- and super-radiant modes; in every case, a very similar behavior was observed. The same method can be applied in order to relate the various coupling parameters with specific physical properties of the system.

The simple but exact formula based on only three coupling parameters reproduces the particular line shapes arising due to interferences between any two resonances, without the help of fitting parameters; this makes it able to predict in what manner the interactions between the parent plasmon modes take place. This formalism hence serves as an essential tool to understand the role played by the various physical properties of the uncoupled system.

## METHODS

Equations 1 that are used throughout this paper in order to produce the Fano line shapes have been first presented in our previous work<sup>18</sup> to which we refer the reader for full details on the derivation.

In the original Fano theory,<sup>12</sup> the interaction  $\langle c|V|d\rangle = \nu(E)$  between a continuum  $|c\rangle$  (CS) and a discrete state  $|d\rangle$  (DS, located at  $E = E_d$ ) creates a mixed state  $|\Psi\rangle$  (MS) which can be written as

$$|\Psi\rangle = \frac{\nu(E)(|d\rangle + |\Omega\rangle) + (E' - E_d - \Delta)|c\rangle}{\sqrt{(E' - E_d - \Delta)^2 + (\Gamma_m(E)/2)^2}} \quad (3)$$

This complex admixture is composed of the two original states spectrally shifted by  $\Delta = \mathcal{P} \int (|\nu(E)|^2)/(E' - E)$  and  $|\Omega\rangle = \mathcal{P} \int (\nu(E)/(E' - E))|c\rangle dE$ , respectively.  $\mathcal{P}$  indicates the "principal part of". In this "configuration interaction", the DS  $|d\rangle$  is by consequence diluted into a finite band of continuum states with half-width  $\Gamma_m(E) = 2\pi|\nu(E)|^2$ . The Fano resonance arises then when the MS  $|\Psi\rangle$  is excited from another initial state  $|i\rangle$  with coupling  $W$ . The resulting interference takes the shape of the well-known Fano profile  $F(\mathcal{L})$ , which is given by the ratio of the probabilities to excite the MS and the unperturbed CS

$$\frac{|i|W|\Psi\rangle|^2}{|i|W|c\rangle|^2} = \frac{(\mathcal{L}+q)^2}{\mathcal{L}^2+1} = F(\mathcal{L}) \text{ with} \quad (4)$$

$$\mathcal{L} = \frac{E - E_d - \Delta}{\Gamma_m(E)/2} \text{ and } q = \frac{\langle \Phi|W|i\rangle}{\pi\nu(E)\langle c|W|i\rangle} \quad (5)$$

$\mathcal{L}$  is the reduced energy and  $1/2\pi q^2$  is the ratio of the probabilities to excite the modified DS  $|\Phi\rangle = |d\rangle + |\Omega\rangle$  and an unperturbed band of CS with width  $\Gamma_m$ . The synthetic form of eq 4 is also grounded by a powerful suit of parameters; however, for an arbitrary continuum, these have no analytic solution. In our particular case, we have considered a plasmonic resonance for the CS defined through a Lorentzian line shape  $\mathcal{L}(E)$  (see eq 2). Taking the DS as origin (*i.e.*,  $E_d = 0$ ) and writing the coupling factors  $\langle c|V|d\rangle = \nu(\mathcal{L}(E))^{1/2}$ ,  $\langle i|W|d\rangle = w$ , and  $\langle i|W|c\rangle = g(\mathcal{L}(E))^{1/2}$ , eqs 5 simplify to eqs 1 that we presented in the first section.<sup>18</sup>

FDTD calculations (solid black lines in every figure and Figure 3, 5a and 6d-g) for the single particle (Figure 2a), the dolmen-like structures (Figures 3–5), and the oligomers (Figure 6) are conducted with a plane wave illumination injected along  $z$  and perfectly matched layers (PML) as external boundaries. Furthermore, meshes have been refined until full convergence and simulations run long enough to resolve all sharp features in the spectra. The infinite arrays (Figure 2b,c) are simulated through periodic boundary conditions along the  $x$  and  $y$  directions around the unit cell  $\Lambda_x \times \Lambda_y$ , and PML are also set along  $z$ .

The Fano interferences studied in the present paper are all revealed in the extinction spectra. These are proportional to the probability of directly exciting the MS with the incident photon  $|i\rangle$  (see eq 4)

$$|i|W|\Psi\rangle|^2 = \frac{(\mathcal{L}+q)^2}{\mathcal{L}^2+1} \times |i|W|c\rangle|^2 = F(\mathcal{L}) \times g^2 \mathcal{L} \quad (6)$$

In presence of absorption, which in quantum mechanics translates as an incoherent process that does not contribute to the interference but adds as a background, the previous

equation reads

$$\begin{aligned} |i|W|\Psi\rangle|^2 &= (F(\mathcal{L}) + A) \times g^2 \mathcal{L} \\ &= g^2 \mathcal{L} \times F(\mathcal{L}) + g^2 \mathcal{L} \times A = F'(E) \end{aligned} \quad (7)$$

Here  $g^2 \mathcal{L}$  is the direct excitation of the bright mode which couples to light and can be related therefore to  $\sigma_{\text{scat}}$  while the nonradiative part given by  $g^2 \mathcal{L} A$  where no interference is present has to be the absorption of the system linked to  $\sigma_{\text{abs}}$ . In summary,  $F'(E)$  is equal to the extinction cross section

$$\text{Ext} = \sigma_{\text{scat}} \times F(\mathcal{L}) + \sigma_{\text{abs}} \quad (8)$$

except for a normalization factor  $C$  that arises because the probability ratio  $F(\mathcal{L})$  (see eq 4) is unitless.

Dashed red curves in Figure 2b,c and Figure 4 are direct applications of eq 8 with the parameters described in the text, none of them being numerically fitted. Even though these profiles are satisfying, some line shapes that display a better accordance (dotted blue lines) with the FDTD results have also been calculated to show how well the simple formulation developed here can reproduce most types of Fano resonances. These are obtained by slowly varying  $\nu$ ,  $E_p$ , and  $\Gamma_p$  for the plasmonic crystals (Figure 2b,c) and  $\nu$ ,  $E_p$ , and  $E_d$  for the dolmen-like structure (Figure 4) in such a way to conserve the profile main features like the extrema position and the peak line width. Details of these changes can be found on each figure.

For the heptamer structure (Figure 6), we have no prior knowledge of the interacting modes, and therefore, we start from the FDTD spectrum (Ext, solid black line in Figure 6a) to retrieve the two original states. This is done by minimizing the error  $|CF(E) - \text{Ext}|$  between eq 7 and the FDTD spectrum and recognizing that the two interfering resonances have Lorentzian line shapes. Here  $C$  is set to  $\max[\text{Ext}]/\max[F(E)]$  and  $A$  in eq 7 is taken as constant; this is only the zero-order Taylor expansion, but higher orders can similarly be considered. Also, the direct excitations of the bright  $|c\rangle$  and the dark  $|d\rangle$  resonances are related to their respective line width, hence  $g = (\Gamma_p/2\pi)^{1/2}$  and  $\nu = (\Gamma_d/2\pi)^{1/2}$ .<sup>18</sup> The parameters  $E_p$ ,  $\Gamma_p$ ,  $E_d$ ,  $\Gamma_d$ ,  $W$ , and  $A$  are unknown, and they are randomly varied around arbitrary starting values. When the error  $|CF(E) - \text{Ext}|$  gets lower than with the starting values, these are updated and the routine started over again. Convergence is generally attained within a few minutes. The optimized  $E_p$ ,  $\Gamma_p$  and  $E_d$ ,  $\Gamma_d$  of the Fano fit (dashed red curve in Figure 6a) give the position and width of, respectively, the extracted bright  $|c\rangle$  (dashed red curve in Figure 6b) and dark  $|d\rangle$  (dashed red curve in Figure 6c) modes that interfere into a Fano resonance.

**Conflict of Interest:** The authors declare no competing financial interest.

**Acknowledgment.** This work was sponsored by the Engineering and Physical Sciences Research Council (EPSRC). V.G. acknowledges funding from the EU through the Marie Curie IEF program.

## REFERENCES AND NOTES

- Giannini, V.; Fernandez-Dominguez, A. I.; Sonnefraud, Y.; Roschuk, T.; Fernandez-Garcia, R.; Maier, S. A. Controlling Light Localization and Light–Matter Interactions with Nanoplasmonics. *Small* **2010**, *6*, 2498–2507.
- Kneipp, K.; Wang, Y.; Kneipp, H.; Perelman, L.; Itzkan, I.; Dasari, R.; Feld, M. Single Molecule Detection Using Surface-Enhanced Raman Scattering (SERS). *Phys. Rev. Lett.* **1997**, *78*, 1667–1670.
- Nie, S.; Emory, S. R. Probing Single Molecules and Single Nanoparticles by Surface-Enhanced Raman Scattering. *Science* **1997**, *275*, 1102–1106.
- Kinkhabwala, A.; Yu, Z.; Fan, S.; Avlasevich, Y.; Muellen, K.; Moerner, W. E. Large Single-Molecule Fluorescence Enhancements Produced by a Bowtie Nanoantenna. *Nat. Photonics* **2009**, *3*, 654–657.
- Noginov, M. A.; Zhu, G.; Belgrave, A. M.; Bakker, R.; Shalae, V. M.; Narimanov, E. E.; Stout, S.; Herz, E.; Suteewong, T.; Wiesner, U. Demonstration of a Spaser-Based Nanolaser. *Nature* **2009**, *460*, 1110–U68.
- Xu, H.; Aizpurua, J.; Käll, M.; Apell, P. Electromagnetic Contributions to Single-Molecule Sensitivity in Surface-Enhanced Raman Scattering. *Phys. Rev. E* **2000**, *62*, 4318–4324.
- Pelton, M.; Aizpurua, J.; Bryant, G. Metal-Nanoparticle Plasmonics. *Laser Photonics Rev.* **2008**, *2*, 136–159.
- Myroshnychenko, V.; Rodriguez-Fernandez, J.; Pastoriza-Santos, I.; Funston, A. M.; Novo, C.; Mulvaney, P.; Liz-Marzan, L. M.; Garcia de Abajo, F. J. Modelling the Optical Response of Gold Nanoparticles. *Chem. Soc. Rev.* **2008**, *37*, 1792–1805.
- Anker, J. N.; Hall, W. P.; Lyandres, O.; Shah, N. C.; Zhao, J.; Van Duyne, R. P. Biosensing with Plasmonic Nanosensors. *Nat. Mater.* **2008**, *7*, 442–453.
- Giannini, V.; Rodriguez-Oliveros, R.; Sánchez-Gil, J. Surface Plasmon Resonances of Metallic Nanostars/Nanoflowers for Surface-Enhanced Raman Scattering. *Plasmonics* **2010**, *5*, 99–104.
- Giannini, V.; Fernandez-Dominguez, A. I.; Heck, S. C.; Maier, S. A. Plasmonic Nanoantennas: Fundamentals and Their Use in Controlling the Radiative Properties of Nanoemitters. *Chem. Rev.* **2011**, *111*, 3888–3912.
- Fano, U. Effects of Configuration Interaction on Intensities and Phase Shifts. *Phys. Rev.* **1961**, *124*, 1866–1878.
- Miroshnichenko, A.; Flach, S.; Kivshar, Y. Fano Resonances in Nanoscale Structures. *Rev. Mod. Phys.* **2010**, *82*, 2257–2298.
- Luk'yanchuk, B.; Zheludev, N. I.; Maier, S. A.; Halas, N. J.; Nordlander, P.; Giessen, H.; Chong, C. T. The Fano Resonance in Plasmonic Nanostructures and Metamaterials. *Nat. Mater.* **2010**, *9*, 707–715.
- Krauth, O.; Fahsold, G.; Pucci, A. Asymmetric Line Shapes and Surface Enhanced Infrared Absorption of CO Adsorbed on Thin Iron Films on MgO(001). *J. Chem. Phys.* **1999**, *110*, 3113–3117.
- Neubrech, F.; Pucci, A.; Cornelius, T. W.; Karim, S.; Garcia-Etxarri, A.; Aizpurua, J. Resonant Plasmonic and Vibrational Coupling in a Tailored Nanoantenna for Infrared Detection. *Phys. Rev. Lett.* **2008**, *101*, 157403.
- Pryce, I. M.; Aydin, K.; Kelaita, Y. A.; Briggs, R. M.; Atwater, H. A. Highly Strained Compliant Optical Metamaterials with Large Frequency Tunability. *Nano Lett.* **2010**, *10*, 4222–4227.
- Giannini, V.; Francescato, Y.; Amrania, H.; Phillips, C. C.; Maier, S. A. Fano Resonances in Nanoscale Plasmonic Systems: A Parameter-Free Modeling Approach. *Nano Lett.* **2011**, *11*, 2835–2840.
- Zhang, S.; Genov, D. A.; Wang, Y.; Liu, M.; Zhang, X. Plasmon-Induced Transparency in Metamaterials. *Phys. Rev. Lett.* **2008**, *101*, 047401.
- Verellen, N.; Sonnefraud, Y.; Sobhani, H.; Hao, F.; Moshchalkov, V. V.; Dorpe, P. V.; Nordlander, P.; Maier, S. A. Fano Resonances in Individual Coherent Plasmonic Nanocavities. *Nano Lett.* **2009**, *9*, 1663–1667.
- Liu, N.; Langguth, L.; Weiss, T.; Kaestel, J.; Fleischhauer, M.; Pfau, T.; Giessen, H. Plasmonic Analogue of Electromagnetically Induced Transparency at the Drude Damping Limit. *Nat. Mater.* **2009**, *8*, 758–762.
- Liu, N.; Weiss, T.; Mesch, M.; Langguth, L.; Eigenthaler, U.; Hirscher, M.; Soennichsen, C.; Giessen, H. Planar Metamaterial Analogue of Electromagnetically Induced Transparency for Plasmonic Sensing. *Nano Lett.* **2010**, *10*, 1103–1107.
- Sherry, L.; Chang, S.; Schatz, G.; Van Duyne, R.; Wiley, B.; Xia, Y. Localized Surface Plasmon Resonance Spectroscopy of Single Silver Nanocubes. *Nano Lett.* **2005**, *5*, 2034–2038.
- Knight, M. W.; Wu, Y.; Lassiter, J. B.; Nordlander, P.; Halas, N. J. Substrates Matter: Influence of an Adjacent Dielectric on an Individual Plasmonic Nanoparticle. *Nano Lett.* **2009**, *9*, 2188–2192.
- Zhang, S.; Bao, K.; Halas, N. J.; Xu, H.; Nordlander, P. Substrate-Induced Fano Resonances of a Plasmonic Nanocube: A Route to Increased-Sensitivity Localized Surface

- Plasmon Resonance Sensors Revealed. *Nano Lett.* **2011**, *11*, 1657–1663.
26. Verellen, N.; Dorpe, P. V.; Vercruysee, D.; Vandenbosch, G. A. E.; Moshchalkov, V. V. Dark and Bright Localized Surface Plasmons in Nanocrosses. *Opt. Express* **2011**, *19*, 11034–11051.
  27. Christ, A.; Ekin, Y.; Solak, H. H.; Gippius, N. A.; Tikhodeev, S. G.; Martin, O. J. F. Controlling the Fano Interference in a Plasmonic Lattice. *Phys. Rev. B* **2007**, *76*, 201405.
  28. Hao, F.; Sonnefraud, Y.; Dorpe, P. V.; Maier, S. A.; Halas, N. J.; Nordlander, P. Symmetry Breaking in Plasmonic Nanocavities: Subradiant LSPR Sensing and a Tunable Fano Resonance. *Nano Lett.* **2008**, *8*, 3983–3988.
  29. Hao, F.; Nordlander, P.; Sonnefraud, Y.; Dorpe, P. V.; Maier, S. A. Tunability of Subradiant Dipolar and Fano-Type Plasmon Resonances in Metallic Ring/Disk Cavities: Implications for Nanoscale Optical Sensing. *ACS Nano* **2009**, *3*, 643–652.
  30. Sonnefraud, Y.; Verellen, N.; Sobhani, H.; Vandenbosch, G. A.; Moshchalkov, V. V.; Van Dorpe, P.; Nordlander, P.; Maier, S. A. Experimental Realization of Subradiant, Super-radiant, and Fano Resonances in Ring/Disk Plasmonic Nanocavities. *ACS Nano* **2010**, *4*, 1664–1670.
  31. Prodan, E.; Radloff, C.; Halas, N.; Nordlander, P. A Hybridization Model for the Plasmon Response of Complex Nanostructures. *Science* **2003**, *302*, 419–422.
  32. Mukherjee, S.; Sobhani, H.; Lassiter, J. B.; Bardhan, R.; Nordlander, P.; Halas, N. J. Fano Resonances: Nanoparticles with Built-in Fano Resonances. *Nano Lett.* **2010**, *10*, 2694–2701.
  33. Mirin, N. A.; Bao, K.; Nordlander, P. Fano Resonances in Plasmonic Nanoparticle Aggregates. *J. Phys. Chem. A* **2009**, *113*, 4028–4034.
  34. Fan, J. A.; Bao, K.; Wu, C.; Bao, J.; Bardhan, R.; Halas, N. J.; Manoharan, V. N.; Shvets, G.; Nordlander, P.; Capasso, F. Fano-like Interference in Self-Assembled Plasmonic Quadrumer Clusters. *Nano Lett.* **2010**, *10*, 4680–4685.
  35. Fan, J. A.; Wu, C.; Bao, K.; Bao, J.; Bardhan, R.; Halas, N. J.; Manoharan, V. N.; Nordlander, P.; Shvets, G.; Capasso, F. Self-Assembled Plasmonic Nanoparticle Clusters. *Science* **2010**, *328*, 1135–1138.
  36. Lassiter, J. B.; Sobhani, H.; Fan, J. A.; Kundu, J.; Capasso, F.; Nordlander, P.; Halas, N. J. Fano Resonances in Plasmonic Nanoclusters: Geometrical and Chemical Tunability. *Nano Lett.* **2010**, *10*, 3184–3189.
  37. Dregely, D.; Hentschel, M.; Giessen, H. Excitation and Tuning of Higher-Order Fano Resonances in Plasmonic Oligomer Clusters. *ACS Nano* **2011**, *5*, 8202–8211.
  38. Hentschel, M.; Saliba, M.; Vogelgesang, R.; Giessen, H.; Alivisatos, A. P.; Liu, N. Transition from Isolated to Collective Modes in Plasmonic Oligomers. *Nano Lett.* **2010**, *10*, 2721–2726.
  39. Alonso-Gonzalez, P.; Schnell, M.; Sarriguarte, P.; Sobhani, H.; Wu, C.; Arju, N.; Khanikaev, A.; Golmar, F.; Albella, P.; Arzubiaga, L.; *et al.* Real-Space Mapping of Fano Interference in Plasmonic Metamolecules. *Nano Lett.* **2011**, *11*, 3922–3926.
  40. Curto, A. G.; Volpe, G.; Taminiau, T. H.; Kreuzer, M. P.; Quidant, R.; van Hulst, N. F. Unidirectional Emission of a Quantum Dot Coupled to a Nanoantenna. *Science* **2010**, *329*, 930–933.
  41. Dregely, D.; Taubert, R.; Dorfmüller, J.; Vogelgesang, R.; Kern, K.; Giessen, H. 3D Optical Yagi-Uda Nanoantenna Array. *Nat. Commun.* **2011**, *2*, 1.
  42. Hentschel, M.; Dregely, D.; Vogelgesang, R.; Giessen, H.; Liu, N. Plasmonic Oligomers: The Role of Individual Particles in Collective Behavior. *ACS Nano* **2011**, *5*, 2042–2050.
  43. Liu, N.; Mukherjee, S.; Bao, K.; Brown, L. V.; Dorfmüller, J.; Nordlander, P.; Halas, N. J. Magnetic Plasmon Formation and Propagation in Artificial Aromatic Molecules. *Nano Lett.* **2012**, *12*, 364–369.
  44. Ameling, R.; Langguth, L.; Hentschel, M.; Mesch, M.; Braun, P. V.; Giessen, H. Cavity-Enhanced Localized Plasmon Resonance Sensing. *Appl. Phys. Lett.* **2010**, *97*, 253116.
  45. Ameling, R.; Dregely, D.; Giessen, H. Strong Coupling of Localized and Surface Plasmons to Microcavity Modes. *Opt. Lett.* **2011**, *36*, 2218–2220.
  46. Artar, A.; Yanik, A. A.; Altug, H. Multispectral Plasmon Induced Transparency in Coupled Meta-Atoms. *Nano Lett.* **2011**, *11*, 1685–1689.
  47. Manjavacas, A.; Abajo, F. J. G. d.; Nordlander, P. Quantum Plexitronics: Strongly Interacting Plasmons and Excitons. *Nano Lett.* **2011**, *11*, 2318–2323.
  48. Shapiro, M. Electromagnetically Induced Transparency with Structured Multicontinua. *Phys. Rev. A* **2007**, *75*, 013424.
  49. Gallinet, B.; Martin, O. J. F. *Ab Initio* Theory of Fano Resonances in Plasmonic Nanostructures and Metamaterials. *Phys. Rev. B* **2011**, *83*, 235427.
  50. Gallinet, B.; Martin, O. J. F. Influence of Electromagnetic Interactions on the Line Shape of Plasmonic Fano Resonances. *ACS Nano* **2011**, *5*, 8999–9008.
  51. López-Tejiera, F.; Paniagua-Domínguez, R.; Rodríguez-Oliveros, R.; Sánchez-Gil, J. A. Fano-like Interference of Plasmon Resonances at a Single Rod-Shaped Nanoantenna. ArXiv e-prints **2011**, DOI: arXiv:1111.3551v2.
  52. Zou, S.; Janel, N.; Schatz, G. Silver Nanoparticle Array Structures That Produce Remarkably Narrow Plasmon Lineshapes. *J. Chem. Phys.* **2004**, *120*, 10871–10875.
  53. Zou, S.; Schatz, G. Silver Nanoparticle Array Structures That Produce Giant Enhancements in Electromagnetic Fields. *Chem. Phys. Lett.* **2005**, *403*, 62–67.
  54. Auguie, B.; Barnes, W. L. Collective Resonances in Gold Nanoparticle Arrays. *Phys. Rev. Lett.* **2008**, *101*, 143902.
  55. Vecchi, G.; Giannini, V.; Rivas, J. G. Surface Modes in Plasmonic Crystals Induced by Diffractive Coupling of Nanoantennas. *Phys. Rev. B* **2009**, *80*, 201401.
  56. Vecchi, G.; Giannini, V.; Rivas, J. G. Shaping the Fluorescent Emission by Lattice Resonances in Plasmonic Crystals of Nanoantennas. *Phys. Rev. Lett.* **2009**, *102*, 146807.
  57. Giannini, V.; Vecchi, G.; Rivas, J. G. Lighting Up Multipolar Surface Plasmon Polaritons by Collective Resonances in Arrays of Nanoantennas. *Phys. Rev. Lett.* **2010**, *105*, 266801.
  58. Zhou, W.; Odom, T. W. Tunable Subradiant Lattice Plasmons by Out-of-Plane Dipolar Interactions. *Nat. Nanotechnol.* **2011**, *6*, 423–427.
  59. Johnson, P.; Christy, R. Optical-Constants of Noble-Metals. *Phys. Rev. B* **1972**, *6*, 4370–4379.
  60. Hutchison, J. A.; O'Carroll, D. M.; Schwartz, T.; Genet, C.; Ebbesen, T. W. Absorption-Induced Transparency. *Angew. Chem., Int. Ed.* **2011**, *50*, 2085–2089.
  61. Yang, Z.-J.; Zhang, Z.-S.; Zhang, L.-H.; Li, Q.-Q.; Hao, Z.-H.; Wang, Q.-Q. Fano Resonances in Dipole-Quadrupole Plasmon Coupling Nanorod Dimers. *Opt. Lett.* **2011**, *36*, 1542–1544.
  62. Palik, E. D. *Handbook of Optical Constants*; Academic Publishers: San Diego, CA, 1984; Vol. 1, p 1297
  63. Halas, N. J.; Lal, S.; Chang, W.-S.; Link, S.; Nordlander, P. Plasmons in Strongly Coupled Metallic Nanostructures. *Chem. Rev.* **2011**, *111*, 3913–3961.
  64. Lassiter, J. B.; Sobhani, H.; Knight, M. W.; Mielczarek, W. S.; Nordlander, P.; Halas, N. J. Designing and Deconstructing the Fano Lineshape in Plasmonic Nanoclusters. *Nano Lett.* **2011**, DOI: 10.1021/nl204303d.